JBC RESEARCH ARTICLE

Monitoring the induction of ferroptosis following dissociation in human embryonic stem cells

Received for publication, December 25, 2021, and in revised form, March 12, 2022 Published, Papers in Press, March 23, 2022,
https://doi.org/10.1016/j.jbc.2022.101855

Shahnaz Babaei-Abraki[1], **Fereshteh Karamali**[2], **and Mohammad Hossein Nasr-Esfahani**[2,*]

From the [1]*Department of Plant and Animal Biology, Faculty of Biological Science and Technology, University of Isfahan, Isfahan, Iran;* [2]*Department of Animal Biotechnology, Cell Science Research Center, Royan Institute for Biotechnology, ACECR, Isfahan, Iran*

Edited by Enrique De La Cruz

Human embryonic stem cells (hESCs) are vulnerable to cell death upon dissociation. Thus, dissociation is an obstacle in culturing, maintaining, and differentiating of hESCs. To date, apoptosis has become the focus of research into the nature of cell death triggered by cellular detachment; it remains baffling whether another form of cell death can occur upon dissociation in hESCs. Here, we demonstrate that iron accumulation and subsequently lipid peroxidation are responsible for dissociation-mediated hESC death. Moreover, we found that a decrease of glutathione peroxidase 4 because of iron accumulation promotes ferroptosis. Inhibition of lipid peroxidation (ferrostatin-1) or chelating iron (deferoxamine) largely suppresses iron accumulation–induced ferroptosis in dissociated hESCs. The results show that P53 mediates the dissociation-induced ferroptosis in hESCs, which is suppressed by pifithrin α. Multiple genes involved in ferroptosis are regulated by the nuclear factor erythroid 2–related factor 2 (Nrf2). In this study, solute carrier family 7 member 11 and glutathione peroxidase 4 are involved in GSH synthesis decreased upon dissociation as a target of Nrf2. In conclusion, our study demonstrates that iron accumulation as a consequence of cytoskeleton disruption appears as a pivotal factor in the initiation of ferroptosis in dissociated hESCs. Nrf2 inhibits ferroptosis *via* its downstream targets. Our study suggests that the antiferroptotic target might be a good candidate for the maintenance of hESCs.

Human embryonic stem cells (hESCs) have unlimited ability to differentiate into almost all types of somatic cells *in vitro* (1, 2), presenting great potential in a wide range of clinical applications, functional genomics, and developmental biology (3–5). hESCs are highly prone to cell death upon matrix and cellular detachment through a process referred to as anoikis (6). To circumvent the problem of anoikis in dissociated hESC culture, many compounds were tested. Of the compounds investigated, Rho kinase (also known as ROCK inhibitor) inhibitor, Y27632, efficiently inhibits cell death after dissociation of hESCs through blocking the Rho/ROCK/myosin cascade, which causes myosin hyperactivation, thereby leading to apoptosis. Though many studies exploring the cell death in hESCs upon dissociation have focused on apoptosis, it is vital to bear in mind that additional modes of cell death may also have occurred. Recent works have reported that epithelial and carcinoma cells become vulnerable to ferroptosis upon matrix detachment (7, 8). Ferroptosis is a type of cell death that is driven by iron and is dramatically distinct from other forms of cell death morphologically and biochemically (9).

Ferroptosis is a consequence of the accumulation of iron, especially Fe^{2+} form, mediatory the generation of alkoxy radical (LO°) through Fenton reaction upon interaction with polyunsaturated fatty acids (PUFAs) to form lipid peroxides (9–12). Our interest in evaluating the ferroptosis pathway in dissociated hESCs was irritated by the exciting data that reported that the primed hESCs have more PUFAs than naïve hESCs (13). Thus, high levels of PUFAs can predispose primed hESCs to ferroptosis, and therefore, hESCs are primarily susceptible to oxidative damage (13), have constitutively activated proapoptotic BAX (14), and fragmented mitochondria (15). Thus, targeting ferroptosis by inhibiting lipid peroxidation (16) and iron chelation (17) may be a promising therapeutic method to counter cell death in hESCs.

It has been reported that ferroptosis is regulated by many genes and molecules. The endogenous antioxidant defense system can be activated to counteract oxidative damage upon initiation of ferroptosis. Nuclear factor erythroid 2–related factor 2 (Nrf2) plays a crucial role in modulating ferroptotic responses through GSH synthesis, which is a cofactor of glutathione peroxidase 4 (GPX4) (16, 18). (19, 20). GPX4 is thought to be a target of various ferroptosis inducers and catalyzes the reduction of lipid and other peroxides (21). Unrepaired lipid peroxides accumulate as a result of the loss of GPX4 activity induced by GSH deficiency, thereby resulting in ferroptosis (22). Thus, it is not surprising that decreasing the cystine uptake by inhibiting cystine/glutamate antiporter system XC^- activity promotes ferroptosis (9). SLC7A11 that encodes a component of the system XC^- is triggered by tumor suppressor protein p53 (23). P53 is a key regulator of ferroptosis and investigated as a regulator of cell death in hESCs in response to DNA damage (14, 24). It has been reported that inhibition of p53 suppresses dissociation-induced apoptosis in hESCs (25).

* For correspondence: Mohammad Hossein Nasr-Esfahani, mh.nasr-esfahani@royaninstitute.org.

Today, it remains blurred whether dissociation mediates ferroptosis in hESCs. For this purpose, we assessed the cell viability, cell proliferation, and colony formation of single hESCs after dissociation in the presence of ferroptosis inhibitors such as deferoxamine (DFO) and ferrostatin-1 (fer-1). These findings give the first information on the ferroptosis pathway in dissociated hESCs as well as a better knowledge of how dissociation induced ferroptosis.

Results

Dissociation induces iron overloading in hESCs

Given that Fe^{2+} has been identified as a critical initiator of ferroptosis, we initially measured intracellular iron after dissociation as a function of time to determine whether dissociation induces ferroptosis in hESCs. The findings from Figure 1*A* revealed that the intracellular iron level of the dissociated hESCs increased rapidly in a time-dependent manner.

The dissociated single hESCs undergo ferroptosis

Given that iron-mediated reactive oxygen species (ROS) production by Fenton reaction promotes lipid peroxidation in the process of ferroptosis (9), we next investigated whether iron overloading induces ferroptosis by analysis of lipid peroxidation using malondialdehyde (MDA) assay. As shown in Figure 1*B*, MDA steadily climbed in dissociated hESCs time-dependently. Another critical ferroptosis regulator is GPX4, which converts lipid peroxide to the corresponding alcohol (26). Apart from that GPX4 buffers lipid peroxidation, we assessed GPX4 activity in dissociated hESCs in a timely fashion, and we observed that it significantly increased, reaching the maximum level upon dissociation, while its activity declined in single cells at 2 to 4 h postdissociation (Fig. 1*C*). The inability to upregulate GPX4 was also demonstrated at the mRNA (Fig. 1*D*) and protein levels 24 h after dissociation (Fig. 1*E*). These findings suggest that iron-dependent cell death is likely occurring in dissociated hESCs.

Ferroptosis inhibitors promote hESC survival and proliferation

Since dissociation of hESCs significantly increased ferroptosis compared with the undissociated colonies, as assessed by the intracellular iron measurement (Fig. 1*A*), to determine whether there is a link between cellular iron and cell death in dissociated hESCs, cell viability was measured using (3-(4,5-dimethylthiazol-2-yl)-2,5-diphenyltetrazolium bromide (MTS) reduction assay. Treatment with various concentrations of

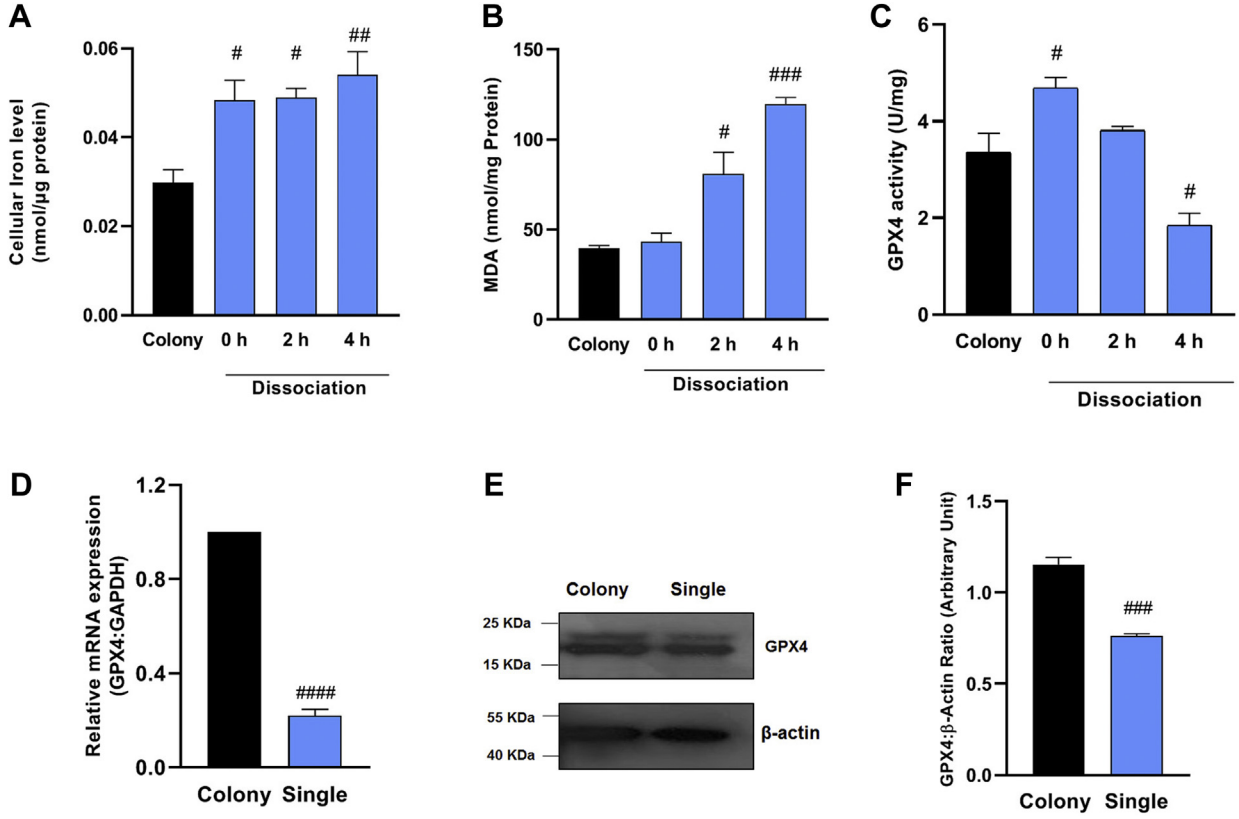

Figure 1. The dissociated single hESCs undergo iron-dependent cell death. *A*, the cellular iron content of hESCs was measured in the colonies and dissociated hESCs, increasing intracellular iron level in a time-dependent manner. *B*, MDA assay was used to quantify lipid peroxidation in the colonies and dissociated hESCs, increasing MDA level in a time-dependent fashion. *C*, GPX4 enzyme activity was assayed in the colonies and dissociated hESCs. *D*, GPX4 mRNA expression between individualized and colonies from hESCs was quantified by qRT–PCR. *E*, GPX4 protein expression was measured using Western blot. *F*, densitometric analysis of GPX4 protein levels; immunoblotting was performed 24 h after dissociation of hESCs. All data are shown as mean ± SEM (n = 3). #$p < 0.05$, ##$p < 0.01$, ###$p < 0.001$, and ####$p < 0.0001$ in comparison to the colony group. GPX4, glutathione peroxidase 4; hESC, human embryonic stem cell; MDA, malondialdehyde; qRT–PCR, quantitative RT–PCR.

ferroptosis inhibitors, including fer-1 (2, 20, and 100 μM) and the iron chelator DFO (1, 10, and 100 μM), did not affect cell survival of dissociated hESCs in comparison to Y-27632-treated hESCs (data not shown). A dose–response curvature of cell viability was observed in response to increasing DFO concentration in combination with Y-27632. Treatment of hESCs with DFO (1 μM) and Y-27632 significantly declined the level of cell death, compared with that observed in the cells exposed solely to Y-27632 (Fig. 2*C*). Moreover, our data showed that a high concentration of DFO (100 μM) reduced hESC viability indicating that iron deprivation also limits hESC survival. As presented in Figure 2*C*, treatment of hESCs by fer-1 (2 and 100 μM) in combination with Y-27632 did not alter cell viability compared with Y-27632-treated cells. The dual treatment of fer-1 (20 μM) with Y-27632 led to a rescue of cell death induced by dissociation in hESCs and thus was used for further investigation. Each inhibitor provided a partial return on its own, and combining both inhibitors (DFO and Y-27632) or (fer-1 and Y-27632) had a synergic effect. Since each of those inhibitors cannot suppress cell death completely, it seems that there may be other forms of cell death that occur in dissociated hESCs. It suggests that anoikis is in the front of the cell death process associated with the dissociation of hESCs, but other forms of cell death, like ferroptosis, are likely involved.

Consistently, fer-1 (20 μM) and DFO (1 μM) in combination with Y-27632 were able to increase the proliferation of hESCs, also they did form dramatically more colonies than Y-27632 did, as assessed by crystal violet staining (Fig. 2*D*). Interestingly, as shown by alkaline phosphatase (ALP) staining, fer-1 (20 μM) and DFO (1 μM) maintained undifferentiated colony morphology of hESCs (Fig. 2, *E* and *F*). These results indicate that iron chelation or inhibition of lipid peroxidation following inhibition of anoikis can prevent ferroptosis as another form of cell death process induced by dissociation in hESCs.

Ferroptosis inhibitors decreased dissociation-induced iron overloading in hESCs

To elucidate whether the observed phenomenon is due to their capacity to deplete iron or to additional characteristics, specific to DFO or fer-1, we measured the iron content in hESCs after exposure to fer-1 (20 μM) or DFO (1 μM) in combination with Y-27632. The results showed that after treatment with DFO and Y-27632, hESCs exhibited significantly lower iron content than the untreated group (Fig. 3*B*). Moreover, we found that dissociation of hESCs increased iron content significantly compared with hESC colonies and that the observed increase in intracellular iron content was prevented by fer-1 in combination with Y-27632. Interestingly, combined treatment of hESCs with DFO or fer-1 with Y-27632 decreased the iron elevation to the control level, whereas Y-27632 alone yielded a partial decrease of iron content compared with the colonies group. Thus, these data imply the involvement of iron in the induction of ferroptosis in dissociated hESCs.

Next, using MDA as a lipid peroxidation marker, we examined whether dual treatment of dissociated hESCs inhibits ferroptosis. A dramatic decrease was seen in MDA level in the presence of DFO (1 μM) in combination with Y-27632 compared with the untreated group. Likewise, a combined treatment of fer-1 (20 μM) and Y-27632 reduced dissociation-induced MDA levels (Fig. 3*C*), and the MDA level reached the level of colonies group in the presence of ferroptosis inhibitors. Moreover, MDA level did not alter in Y-27632-treated cells compared with untreated cells showing the inability of Y-27632 to decrease iron content and the subsequent effect on lipid peroxidation. Because of the regulatory impact of ferroptosis inhibitors on GPX4, we next measured GPX4 activity in the presence of ferroptosis inhibitors. GPX4 activity was increased by DFO (1 μM), indicating the role of iron chelation in sustaining the cell in a redox balance (Fig. 3*D*). Fer-1 (20 μM) treatment of dissociated hESCs showed an increase in GPX4 activity compared with untreated cells. Our results showed that the increase of MDA upon dissociation is likely reduced by ferroptosis inhibitors through GPX4 activation.

P53 mediates the dissociation-induced ferroptosis in hESCs

Emerging evidence suggested that reducing cystine uptake through repression of SLC7A11 (Fig. 4*A*) makes cells vulnerable to ferroptosis (27). On the other side, hESCs express high levels of p53 protein in the cytosol under standard culture conditions (24, 28). Based on the exciting literature, we embarked on deciphering the molecular mechanism by which dissociation induces ferroptosis in hESCs. To clarify whether dissociation-induced ferroptosis in hESCs is mediated by p53, we determined mRNA levels of p53 by quantitative RT–PCR (qRT–PCR). As shown in Figure 4*B*, p53 increased in dissociated hESCs compared with the colonies group. Then to determine whether p53 induces ferroptosis through inhibiting cystine import, the mRNA level of SLC7A11 was measured. We observed that mRNA levels of SLC7A11 markedly decreased in dissociated hESCs compared with the undissociated colonies group (Fig. 4*B*). Then, we examined the change expression of p53 time-dependently using a Western blot technique. Interestingly, the expression of p53 increased following dissociation (Fig. 4*C*). We observed that dissociation of hESCs increased p53 protein level in a timely fashion and that the observed increase in p53 expression was prevented by pifithrin α (Pft-α, p53 inhibitor). Treatment of hESCs with Pft-α (10 μM) inhibited the increase in the p53 level after dissociation (Fig. 4*E*). These data suggest that p53 mediates the dissociation-induced ferroptosis in hESCs. To investigate the role of p53 in hESC dissociation-induced ferroptosis, we also examined the effects of Pft-α on the ferroptosis pathway. As presented in Figure 4*G*, GPX4 and xCT (the cystine–glutamate antiporter) expressions were downregulated by Pft-α, indicating that p53 mediates the dissociation-induced ferroptosis pathway.

Ferroptosis inhibitors modulate p53 level in dissociated hESCs

Next, the mechanism by which DFO and fer-1 prevent ferroptosis was investigated. To this end, we examined mRNA

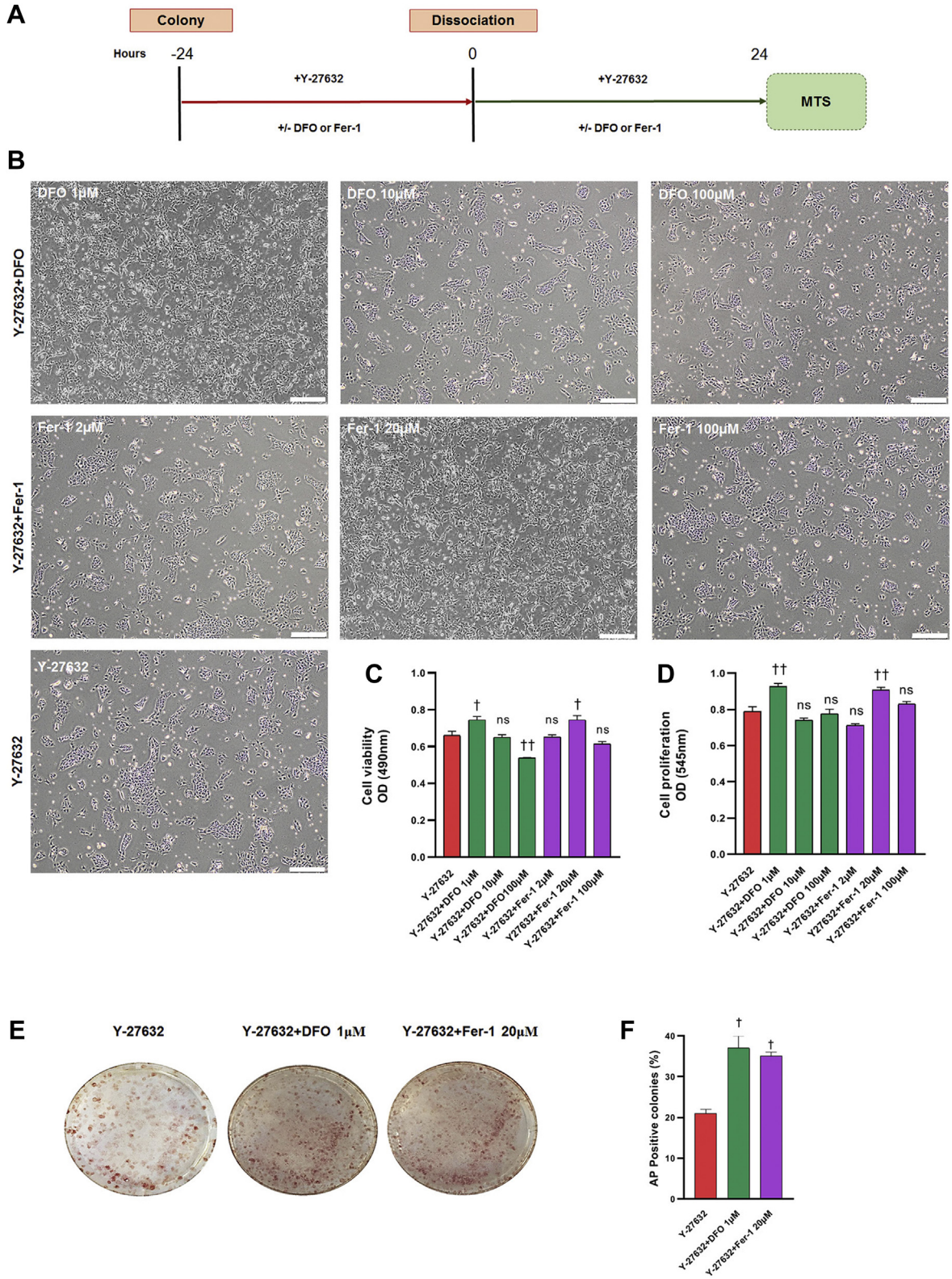

Figure 2. Ferroptosis inhibitors promote hESC survival and proliferation. *A*, diagram of MTS assay. *B*, phase images of hESCs treated with Y-27632, or 1, 10, and 100 μM DFO in combination with Y-27632 or 2, 20, and 100 μM fer-1 in combination with Y-27632. The scale bar represents 200 μm. *C*, viability of hESCs exposed to (1, 10, and 100 μM) DFO in the presence of Y-27632 or (2, 20, and 100 μM) fer-1 in combination with Y-7632 was analyzed using MTS assay. *D*, graphic quantification of crystal violet staining of hESC colonies showing dramatic differences in colony formation in the presence of (1 μM) DFO along with Y-27632 and (20 μM) fer-1 in combination with Y-27632 compared with Y-27632 treated alone. *E*, photograph of alkaline-positive staining of hESCs exposed to (1 μM) DFO in the presence of Y-27632 or (20 μM) fer-1 in combination with Y-7632. *F*, the ratio of ALP-positive colonies produced per seeded hESCs was used to assess cloning efficiency. The optimum dose of DFO (1 M) or fer-1 (20 M) was employed in combination with Y-27632 for the first 24 h following culturing of dissociated single hESCs until colonies formed. The cells were cultured for 8 days. All data are shown as mean ± SEM (n = 3). †$p <$ 0.05, ††$p <$ 0.01 compared with the Y-27632 group. ALP, alkaline phosphatase; DFO, deferoxamine; Fer-1, ferrostatin-1; hESC, human embryonic stem cell; MTS, (3-(4,5-dimethylthiazol-2-yl)-2,5-diphenyltetrazolium bromide.

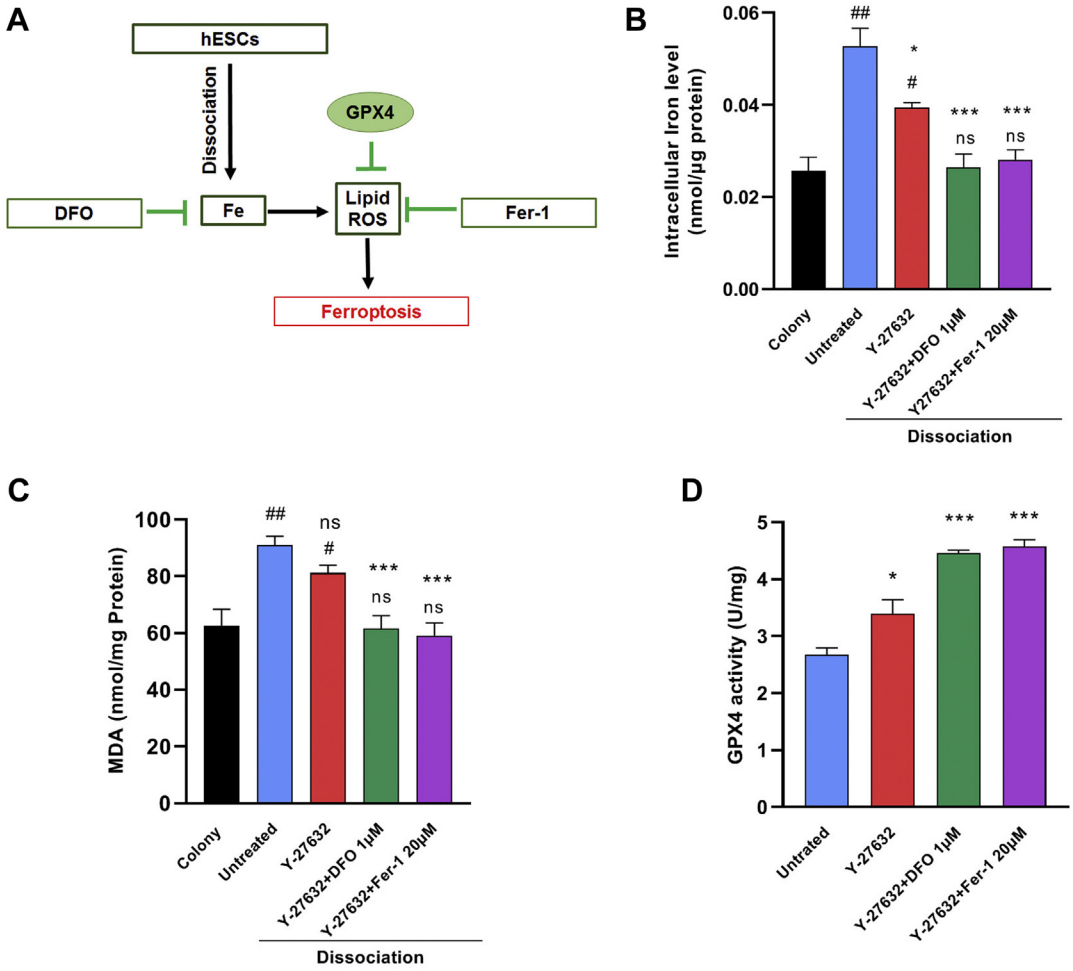

Figure 3. Ferroptosis inhibitors decreased dissociation-induced iron overloading in hESCs. *A*, schematic figure showing the ferroptosis pathway and the functions of relevant inhibitors. *B*, intracellular iron level of hESCs treated with 1 μM of DFO or 20 μM of fer-1 along with Y-27632 for 4 h. *C*, MDA assay was used to detect lipid peroxidation in the presence of DFO (1 μM) or fer-1 (20 μM) along with Y-27632. *D*, GPX4 enzyme activity was assayed in the presence of DFO (1 μM) or fer-1 (20 μM) along with Y-27632 in dissociated hESCs. All data are shown as mean ± SEM (n = 3). *$p < 0.05$, ***$p < 0.001$ compared with the untreated group and #$p < 0.05$, ##$p < 0.01$ compared with colonies. DFO, deferoxamine; Fer-1, ferrostatin-1; GPX4, glutathione peroxidase 4; hESC, human embryonic stem cell; MDA, malondialdehyde.

levels of P53 by qRT–PCR in DFO and fer-1-treated cells in combination with Y-27623. We found that not only Y-27632 alone but also in combination with DFO decreased p53 mRNA level compared with untreated cells (Fig. 4*I*). To further support this conception, we determined the expression of p53 using Western blot analysis. As revealed in Figure 4*J*, a drastic reduction of p53 expression was observed in the presence of fer-1 or DFO in combination with Y-27632. Correspondingly, the expression of p53 was downregulated in the DFO or fer-1 treatment group indicating the rescue effect of ferroptosis inhibitors in dissociation-induced cell death in hESCs.

Nrf2 pathway and its downstream targets antagonize iron overloading to promote resistance of hESCs to ferroptosis in the dissociated single hESCs

Previous studies have demonstrated that Nrf2 preserves the ability of cells to counteract ferroptosis through its downstream GPX4 and SLC7A11, which are necessary for GSH synthesis (Fig. 5*A*) (29). At first, we measured GSH level in the presence of ferroptosis inhibitors. Our results from Figure 5*B* revealed that GSH content increased in the presence of ferroptosis inhibitors (fer-1 or DFO in combination with Y-27632) compared with untreated cells. To elucidate whether ferroptosis inhibitors (DFO and fer-1) suppress cell death in dissociated hESCs through Nrf2, we were inspired to evaluate the Nrf2 pathway. Notably, Nrf2 expression is also downregulated upon dissociation in hESCs (Fig. 5*C*). To determine the modification of Nrf2 level in dissociated hESCs, cells were exposed to 1 μM DFO or 20 μM fer-1 in combination with Y-27632 followed by qRT–PCR. Our results from qRT–PCR showed that Y-27632 did not alter Nrf2 mRNA expression in comparison to untreated cells (Fig. 5*D*). However, the ability to upregulate Nrf2 was found at the mRNA expression (Fig. 5*D*) as well as protein expression in the presence of fer-1 in combination with Y-27632 (Fig. 5*G*). Furthermore, we observed an increase of Nrf2 in DFO-exposed hESCs compared with untreated cells. To confirm the effect of ferroptosis inhibitors on the Nrf2 pathway, we evaluated the downstream targets of Nrf2. A severe elevation in SCL7A11

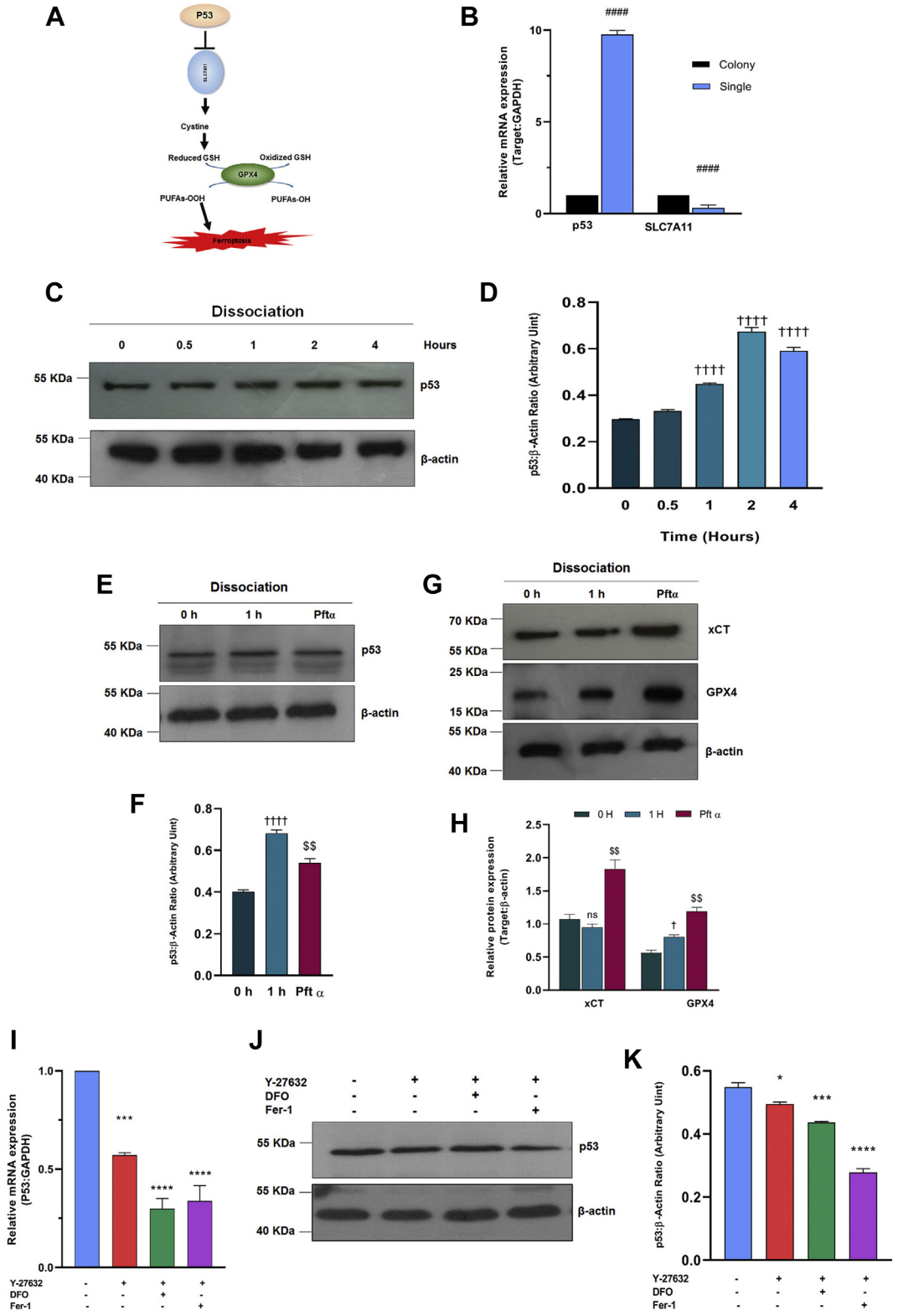

Figure 4. p53 stimulates the dissociation-induced ferroptosis in hESCs. *A*, schematic figure showing p53-mediated activation of ferroptosis. *B*, p53 and SLC7A11 mRNA expression was determined by qRT–PCR in dissociated hESCs and colony culture. *C*, Western blot analysis of p53 expression in dissociated hESCs time-dependently. *D*, densitometric analysis of p53 protein levels; immunoblotting was performed 0–4 h after dissociation of hESCs. *E*, Western blot analysis of p53 expression in hESCs treated with Pft-α (10 μM). Dissociated cells were treated with Pft-α (10 μM) for 2 h and then dissociated into single cells and cultured for 1 h. *F*, densitometric analysis of p53 protein levels. *G*, Western blot analysis of xCT and GPX4 expression in hESCs treated with Pft-α (10 μM). *H*, densitometric analysis of xCT and GPX4 protein levels. *I*, mRNA expression of p53 was assessed by qRT–PCR in the presence of DFO (1 μM) or fer-1 (20 μM) along with Y-27632 in dissociated hESCs. GAPDH was used as a loading control. *J*, Western blot analysis of p53 expression in hESCs treated with DFO (1 μM) or fer-1 (20 μM) in combination with Y-27632. *K*, densitometric analysis of p53 protein levels; immunoblotting was performed 4 h after dissociation of hESCs. β-actin was used as an internal control. All the experiments were done 4 h after the dissociation of hESCs. All data are shown as mean ± SEM (n = 3). *$p < 0.05$, ***$p < 0.001$, and ****$p < 0.0001$ compared with the untreated group and, ####$p < 0.0001$ in comparison to colonies.

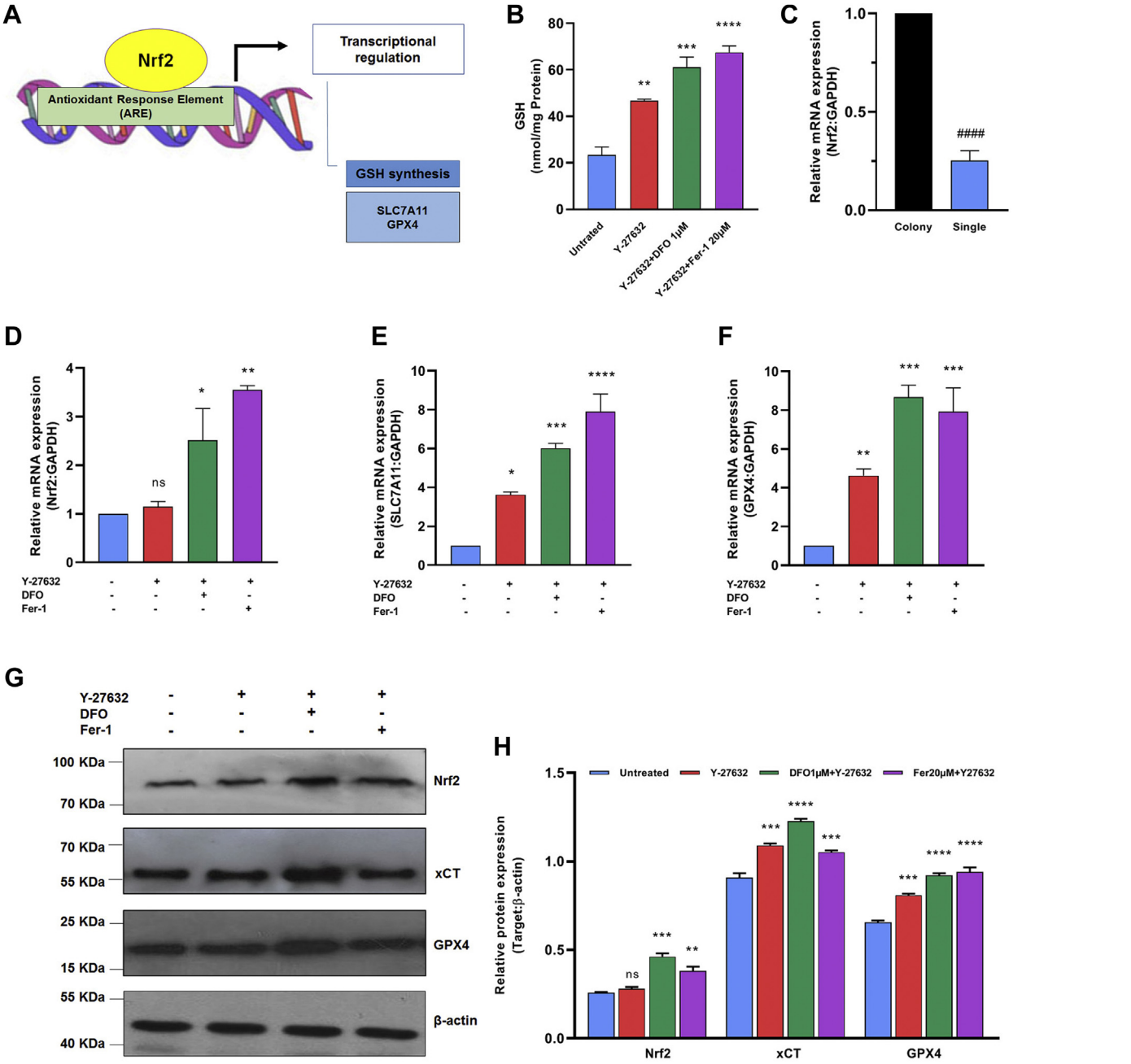

Figure 5. Nrf2 and its downstream targets (SLC7A11 and GPX4) promote the resistance of hESCs to ferroptosis in the dissociated single hESCs. *A*, schematic figure showing the role of Nrf2 in GSH synthesis through its target genes. *B*, GSH content was measured in the presence of DFO (1 μM) or fer-1 (20 μM) along with Y-27632 in dissociated hESCs. *C*, qRT–PCR was applied to measure Nrf2 mRNA expression in dissociated hESCs and colonies culture. *D*, Nrf2 mRNA expression was assessed by qRT–PCR in the presence of DFO (1 μM) or fer-1 (20 μM) along with Y-27632 in dissociated hESCs. *E*, expression of SLC7A11 was assessed by qRT–PCR in the presence of DFO (1 μM) or fer-1 (20 μM) along with Y-27632 in dissociated hESCs. *F*, qRT–PCR was applied to analyze GPX4 expression in the presence of DFO (1 μM) or fer-1 (20 μM) in combination with Y-27632 in dissociated hESCs. GAPDH was used as a loading control. *G*, Western blot analysis of Nrf2, xCT, and GPX4 expression in hESCs treated with DFO (1 μM) or fer-1 (20 μM) along with Y-27632. β-actin was used as an internal control. All the experiments were performed 4 h after the dissociation of hESCs. *H*, densitometric analysis of Nrf2, SLC7A11, and GPX4 protein levels; immunoblotting was performed 4 h after dissociation of hESCs. All data are shown as mean ± SEM (n = 3). *$p < 0.05$, **$p < 0.01$, ***$p < 0.001$, and ****$p < 0.0001$ compared with the Y-27632 group and ###$p < 0.001$ compared with colonies. DFO, deferoxamine; fer-1, ferrostatin-1; GPX4, glutathione peroxidase 4; hESC, human embryonic stem cell; Nrf2, nuclear factor erythroid 2–related factor 2; qRT–PCR, quantitative RT–PCR; xCT, the cystine–glutamate antiporter.

and GPX4 mRNA levels was observed (Fig. 5, *E* and *F*) in the presence of Y-27632. Moreover, we established that SCL7A11 and GPX4 mRNA levels increased in the presence of ferroptosis inhibitors, which were also confirmed by our data from Western blot (Fig. 5*G*). As quantified in Figure 5*H*, we found that the xCT increased by 1.15-fold in the presence of

††††$p < 0.0001$ compared with 0 h. $$$p < 0.01$ compared with 1 h. Fer-1, ferrostatin-1; GPX4, glutathione peroxidase 4; hESC, human embryonic stem cell; Pft-α, pifithrin α; qRT–PCR, quantitative RT–PCR; xCT, the cystine–glutamate antiporter.

fer-1 in combination with Y-27632 compared with the untreated group. The same results were obtained in DFO-treated hESCs in the xCT expression, showing its critical role in sustaining the cells in balance. Therefore, iron overload should be the key reason for cell death in hESCs upon dissociation, which was rescued by ferroptosis inhibitors through the Nrf2 pathway.

Discussion

In this study, we attempt to understand whether ferroptosis is taking place upon dissociation in hESCs. In this type of cell death, lipid peroxides exceed threshold levels as a result of iron accumulation (30). Our results revealed that iron overloading was observed following dissociation in hESCs, indicating the critical role of iron homeostasis in hESC survival as observed in our result of cell viability data. This observation was in line with the previous study demonstrating that iron overloading restricts the self-renewal of hPSCs *via* ROS generation, consequently leading to DNA damage (31). We showed that DFO, a specific iron chelator, in combination with Y-27632 restores dissociation-induced cell death, demonstrating an involvement of iron to precede ferroptosis in individualized hESCs. Following the previous study (32), we also found that unlike a low concentration of DFO (1 μM), a high concentration of DFO (100 μM) reduces hESC survival indicating that iron deprivation limits hESC maintenance and survival. In addition, we showed that treatment with fer-1 and DFO in the presence of Y-27632 improves cellular proliferation and also colony formation assessed by ALP staining. Therefore, we concluded that the following anoikis, ferroptosis, also complement the process of cell death upon dissociation of hESCs.

Considering that unchelated iron can result in lipid peroxides and subsequent ferroptosis (27, 33), we measured lipid peroxidation, which has been shown to degrade into hydroxy fatty acids or reactive aldehydes, such as MDA (34). Our results evidenced that iron accumulation promotes ferroptosis *via* the production of lipid peroxides as assessed by MDA being in line with Yang *et al.* (11). We also indicated that the release of iron upon dissociation in hESCs could induce ferroptosis, as treatment with ferroptosis inhibitor before and following dissociation in hESCs reduce iron content as well as MDA level revealing new information about cell death pathways in individuated hESCs.

Previous studies demonstrated that upon dissociation, hESCs undergo massive cell death through a process termed anoikis (35–37). Although the initiation signal of anoikis is not yet vibrant, cytoskeleton disruption has been identified in anoikis (38). The loss of E-cadherin-dependent intercellular contact is considered a pivotal initiator of dissociation-induced actomyosin hyperactivation and membrane blebbing, consequently cell death (36). To reduce anoikis, ROCK inhibitor (Y-27632) has been implemented and has become part of the routine protocol for dissociation and passaging of hESCs. In this study, we found that Y-27632 could partially restore iron content compared with untreated cells indicating treatment by Y-27632 plus ferroptosis inhibitors had a synergistic effect on ferroptosis suppression compared with Y-27632 alone. Furthermore, Y-27632 on its own does not reduce MDA following dissociation. Thus, these data suggest that, in addition to anoikis, ferroptosis is also involved in the cell death mechanism following hESC dissociation. In agreement with our results, Brown *et al.* (8) found that ferroptosis could occur in epithelial and carcinoma cells upon matrix detachment. Furthermore, perturbation of the cytoskeleton has been linked to an increase in intracellular iron and promotes ferroptosis, as reported by Sun *et al.* (39) They evidenced that actin cytoskeleton disruption in HeLa cells increased intracellular iron and lipid ROS production, consequently promoting ferroptosis. Therefore, it can be concluded that the dissociation of hESCs leads to the destruction of the cell–cell junction and also cytoskeleton, consequently resulting in the accumulation of Fe^{2+}, which promotes ferroptosis *via* lipid peroxidation (Fig. 6) (40).

To have more insight on ferroptosis associated with dissociation of hESCs, we piqued to assess the expression of cellular markers involved in ferroptosis, including GPX4, SLC7A11, Nrf2, and p53. Since the loss of GPX4 activity has been reported to induce ferroptosis (20), it is not surprising that decreasing the GSH content as a consequence of inhibiting system XC^- activity also promotes ferroptosis (9). Ferroptosis has been demonstrated to be a vital function of tumor suppression by p53, a negative regulator of SLC7A11 (27, 41, 42). Here, we showed that upon dissociation of hESCs, p53 increased with time, which was reversed by administration of p53 inhibitor (Pft-α). Moreover, our study showed that inhibition of p53 decreased xCT and GPX4 expression indicating the role of p53 in promoting ferroptosis. Inconsistent with our results, Zhang *et al.* (28) reported that dissociation-induced apoptosis of hESCs can be diminished by Pft-α. We further showed that Y-27632 in combination with DFO and fer-1 decreased p53 mRNA level compared with untreated cells. Recently, it has been reported that p53 maintains iron homeostasis (43). Moreover, it has been reported that significant elevation of serum iron levels is associated with $p53^{-/-}$ but not $p53^{+/+}$ mice, indicating the role of p53 in iron hemostasis (44). Thus, it seems that excess iron upon dissociation in hESCs is likely to be related to p53 upregulation and subsequent cell death as confirmed in ovarian granulosa cells (45).

Nrf2 regulates the expression of a variety of proteins, and enzymes inhibit lipid peroxidation and the onset of ferroptosis (46). Nrf2 upregulates the system XC^-, which provides cysteine for GSH and consequently sustains the activity of GPX4 (47, 48), which reduces lipid peroxides to lipid alcohols (LOOH) restoring cell membrane integrity (34, 49). Our study showed that the amount of GPX4 activity initially increased and subsequently significantly decreased in comparison with the control group, indicating that following dissociation, hESCs aim to rescue lipid peroxidation but fail to do so as no reduction was observed in MDA level; with progression in time from dissociation, this ability is also lost, which consequently results in iron-induced cell death or ferroptosis (50, 51). Moreover, a dramatic reduction in Nrf2 was seen upon dissociation, indicating the requirement of Nrf2 in protecting

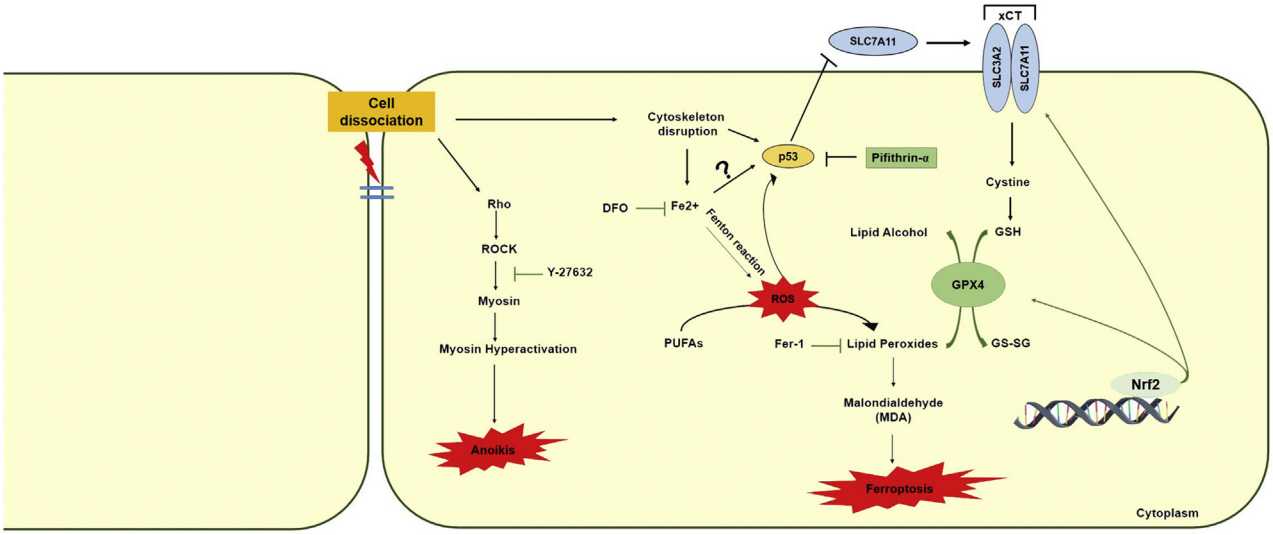

Figure 6. Overview of cell death in dissociated hESCs. After hESC dissociation, the Rho/ROCK signaling pathway is activated, which leads to anoikis. Inhibition of Rho/ROCK signaling *via* Y-27632 suppresses hESC death; however, cloning efficiency is still low in many cases. Moreover, dissociation results in cytoskeleton perturbation leading to iron accumulation, which forms hydroxyl/peroxyl radicals *via* the Fenton reaction. Hydrogen atoms from polyunsaturated fatty acids (PUFAs) combine to form a lipid radical, which interacts quickly with oxygen to form lipid peroxide. This process can be inhibited by ferrostatin-1 (fer-1). Lipid peroxides can be degraded into reactive aldehydes, such as malondialdehyde (MDA). Decreased iron overload by iron chelators such as deferoxamine (DFO) inhibits dissociation-induced ferroptosis in hESCs. Activation of p53 is required for ferroptosis in dissociated hESCs. Direct transcriptional suppression of SLC7A11, a major component of system XC^-, is required for ferroptosis. The xCT antiporter (consisting of two subunits SLC7A11 and SLC3A2) is responsible for maintaining redox homeostasis through importing cystine, subsequently GSH synthesis. Reduced GSH is converted to oxidized GSH by glutathione peroxidase 4 (GPX4), which also reduces lipid hydroperoxides to their corresponding alcohols or free hydrogen peroxide to water. Through the elevation of SLC7A11 and GPX4 expression, which enables cystine intracellular uptake, Nrf2 is thought to be a critical negative regulator of ferroptosis. hESC, human embryonic stem cell; Nrf2, nuclear factor erythroid 2–related factor 2; ROCK, Rho kinase.

hESCs against ferroptosis (52, 53). Because of the low activity of cysteine transport in hESCs (54), activation of Nrf2, subsequently upregulation of xCT expression, can enable cells to counteract oxidative damage (55), which has been revealed in the previous study through the addition of *N*-acetylcysteine (56). Western blot results showed that Nrf2 expression as well as its downstream targets increased in the presence of ferroptosis inhibitors, indicating Nrf2 stimulates SLC7A11 expression subsequently promoting intracellular cystine uptake for GSH synthesis as a cofactor of GPX4 (18). This observation is in affirmation with our data from GPX4 activation in the presence of DFO and fer-1, a representative that the response of dissociated hESCs to ferroptosis is primarily determined by GPX4 activity. Our data from GSH content confirmed that ferroptosis inhibitors provide GSH for cell survival. Although our results from qRT–PCR and Western blot showed that Y-27632 did not alter Nrf2 expression compared with untreated cells, it seems that Y-27632 alone protects dissociated hESCs by counteracting other mechanisms including anoikis. In addition, Y-27632 on its own does not reduce MDA and iron level following dissociation, further reiterating anoikis and ferroptosis also likely to be two independent mechanisms involved in cell death following hESC dissociation. In summary, these findings demonstrated that Nrf2 could improve the redox balance by enhancing cysteine uptake to maintain GPX4 activity and counteract iron-dependent cell death (18, 54, 55, 57).

In summary, to our knowledge, our research is the first to report that independent of anoikis, iron accumulation cause ferroptosis in hESCs upon dissociation. Iron accumulation has been reported to associate with cellular damage leading to lipid peroxidation and consequently ferroptosis (9), and iron accumulation has been shown to reduce cellular damage (31, 58). Although our study showed that inhibition of p53 modulates cell death in dissociated hESCs. Excess Fe^{2+} has been reported that leads to p53 activation (45); it remains unclear whether p53 activation is the reason or the consequence of iron accumulation in dissociated hESCs. Our data revealed that Nrf2 activation resists dissociated hESCs against ferroptosis through upregulation of its downstream targets SLC7A11 and GPX4. Thus, Nrf2 activation could be a powerful anti-ferroptotic target for the maintenance of the genetic integrity of hESCs through the use of iron chelator (DFO), an inhibitor of lipid peroxidation (fer-1), and Nrf2 activators.

Experimental procedures

Cell culture

Experiments were done with the hESC line (RH6) (59). hESCs were grown on a feeder layer of mouse embryonic fibroblast cells, which were inactivated with 10 μg/ml mitomycin C. hESCs were fed daily with Dulbecco's modified Eagle's medium/F-12 (Gibco; catalog no.: 21331-020) complemented with 20% knockout serum replacement (Gibco; catalog no.: 10828-028), 1% nonessential amino acids (Gibco; catalog no.: 11140-035), 0.1 mM β-mercaptoethanol (Sigma–Aldrich; catalog no.: M3148), 1% antibiotic mixture comprising 100 units/ml penicillin and 100 μg/ml streptomycin (Gibco; catalog no.: 15070063), insulin–transferrin–selenite (Gibco; catalog no.: 41400-045), 2 mM L-glutamine

(Gibco; catalog no.: 25030-024), and 100 ng/ml basic fibroblast growth factor (Royan Institute) in an ideal atmosphere of 37 °C with 5% CO_2 air-humidified incubator. The growth medium was treated daily with a 10 μM ROCK inhibitor (Y-27632; Calbiochem; catalog no.: 688000), and hESC colonies were passaged by collagenase IV (Gibco; catalog no.: 17104-019) in Dulbecco's modified Eagle's medium/F12 for 7 min. For dissociation into a single cell, hESCs were washed with PBS^- and then treated with accutase (Millipore; catalog no.: SCR005) at 37 °C for 3 min and harvested by pipetting, then cultured to Matrigel-coated (Sigma–Aldrich; catalog no.: E1270) dishes.

Measurement of cell viability

To assess the survival of dissociated hESCs in the presence of ferroptosis inhibitors, a conventional MTS reduction assay was performed. In this chromogenic experiment, tetrazolium is reduced by viable cells. Described briefly, dissociated hESCs were cultured into the Matrigel-coated 96-well plate at the density of 35×10^4 cells/cm^2 for 72 h. Then cells were exposed to various concentrations of (2, 20, and 100 μM) fer-1 (Cayman Chemical; catalog no.: 17729) or (1, 10, and 100 μM) DFO (Sigma–Aldrich; catalog no.: D9533). After 24 h, MTS was added to each well and then incubated for 4 h at 37 °C in the darkness; absorbance was measured at 490 nm using a microplate reader (Awareness).

Cell proliferation assay

To investigate cell proliferation, crystal violet staining was used. In short, the hESCs were dissociated into single cells and transferred to Matrigel-coated dishes. Dissociated hESCs were exposed to different concentrations (2, 20, and 100 μM) of fer-1 or (1, 10, and 100 μM) DFO. After colony formation, cells were rinsed in PBS and fixed with 70% methanol. Fixed cells were stained with 0.4% crystal violet solution for 30 min after being washed three times in PBS, and images were acquired using a digital camera at 1× magnification (D7000; Nikon). Following treatment with 500 μl 10% acetic acid, the absorbance was detected using a microplate reader (Awareness).

Colony formation

The dissociated hESCs were cultured in a Matrigel-coated 6-well plate at a low density of 500 cells/cm^2 in a complete culture medium. Dissociated hESCs were treated with the optimum dose of DFO (1 M) or fer-1 (20 M) by adding Y-27632 for the first 24 h followed by culturing of dissociated single hESCs until colonies formed. The medium was changed daily. After 8 days of culture, the hESC colonies were visualized by ALP staining using the leukocyte ALP kit (Sigma; catalog no.: 86R). Cloning efficiency of dissociated single hESCs ([number of ALP-positive colonies/number of seeded cells] × 100) by analyzing the numbers of feeder-independent colonies.

Cellular iron content assay

Intracellular iron was assessed using an iron assay kit (catalog no.: K390-100; BioVision). In brief, hESCs were washed with PBS and lysed with iron assay buffer at appropriate times. Cells were harvested by centrifuging at 16,000*g* for 10 min to remove insoluble materials. Then 50 μl sample was added to a 96-well plate to bring in a final volume of 100 μl/well with assay buffer. To reduce iron (III) to iron (II), 5 μl of iron reducer was added following incubation for 30 min at 25 °C. Finally, an iron probe was added and incubated for 30 min at 25 °C in darkness. Using a microplate reader, the absorbance was measured at 593 nm. Iron contents were normalized to protein concentration.

Measurement of lipid peroxidation

The Nalondi Lipid Peroxidation (MDA) assay kit (Navandsalamat; catalog no.: NS-15022) was used to measure lipid peroxidation according to the manufacturer's guidelines. Briefly, cells were lysed with lysis buffer and reacted with thiobarbituric acid followed by centrifuging at 13,000*g* for 3 min. In the assay, the working solution was added to the sample, and then the samples were boiled in a boiling water bath (95 °C) for 45 min. Then, samples were centrifuged at 3000*g* for 15 min. Finally, using a microplate reader, the purple color absorbance was measured at 550 nm. Lipid peroxidation levels were normalized to protein concentration.

Measurement of GPX4 activity

GPX4 activity was measured using Nagpix GPX activity test kit (Navandsalamat; catalog no.: NS-15082). Briefly, cells were lysed with assay buffer after being washed three times with cold PBS. The cells were then harvested after 15 min of centrifugation at 9000*g*. A 50 μl sample was added to a 96-well plate and was brought to a volume of 90 μl/well with reagent 1, and samples were incubated at room temperature for 15 min. About 10 μl of reagent 2 was added to start a reaction. Using a microplate reader, the absorbance was measured at 340 nm twice; (first time) at time 0 and (second time) at time 15 min. GPX4 activity was normalized to protein concentration.

Measurement of GSH levels

The concentration of GSH was determined in whole cell lysates using the dithionitrobenzoic acid method at 412 nm (60). In brief, cells were lysed with 10% tricolor acetic acid and homogenized through sonication. Then, 0.1 ml supernatant was mixed with dithionitrobenzoic acid in 0.1 M potassium phosphate buffer with 5 mM ethylenediaminetetraacetic acid. For this assessment, the absorbance of different samples was read by a spectrophotometer device. GSH concentrations were expressed as nanomole/milligram protein.

RNA extraction and real-time qRT–PCR

RNeasy Kit (Qiagen; catalog no.: 74004) was used to extract total RNA from hESCs. RNA concentrations were determined by Nanodrop (Thermo Fisher Scientific). Complementary DNA was synthesized from total RNA using Reverse Transcription System Kit (Biotech rabbit; catalog no.: BR0400601) as described in the manufacturer's protocol. Applied

Biosystems step one plus Real-Time PCR System (Thermo Fisher Scientific) was used to carry out real-time qRT–PCR, using SYBR green Gene Expression Master Mix (TaKaRa; catalog no.: PR820Q). Beacon Designer software (version 7.2) as obtained from Metabion (Planegg/Steinkirchen) was used to design real-time–specific primer pairs. All measurements were performed in three biological replicates. The results were normalized to GAPDH, and △△Ct method was selected to calculate the relative expression of genes in comparison to the control groups (61). The following primers were used to determine ferroptosis in hESCs:

PCR primers: For qRT–PCR: human GAPDH, forward: CCACTCCTCCACCTTTGACG, reverse: CCACCACCC TGTTGCTGTAG; human p53, forward: GCTGGTTAGGT AGAGGGAGTTG, reverse: GTGTGGGATGGGGTGAGA TTTC; human Nrf2, forward: TCACAAGAGATGAACTT AGGGCAA, reverse: AGCCACTTTATTCTTACCCCTC; human GPX4, forward: GCCTTCCCGTGTAACCAGT, reverse: TTTCCCAGGATGCCCTTGCC; human SLC7AL11, forward: TGTCTCCAGGTTATTCTATGTTG, reverse: CCA GAGAAGAGCATTATCATTG.

Protein extraction and Western blotting

At the given time points, cells were lysed using TRIzol reagent (Ambion; catalog no.: 15596-08) according to the manufacturer's instructions to obtain protein. Bradford's method was employed in the process of protein content concentration (62). A standard plot was generated using bovine serum albumin. We separated the protein using 10% SDS-PAGE followed by electrotransfer onto a polyvinylidene fluoride membrane (Bio-Rad; catalog no.: 162-0176). Then, the membranes were blotted overnight at 4 °C in blocking buffer (1× Tris-buffered saline containing 5% w/v skim milk, 0.1% Tween-20). Membranes were probed with antibodies against Nrf2 (1:2000 dilution; Abcam; catalog no.: ab62352), GPX4 (1:500 dilution; Abcam; catalog no.: ab125066), p53 (1:200 dilution; Cell Signaling; catalog no.: 2524), SCL7A11 (1:500 dilution; Abcam; catalog no.: ab37185), and β-actin (1:200 dilution; Santa Cruz; catalog no.: SC47778) for 2 h at room temperature. Signals derived from appropriate horseradish peroxidase–conjugated secondary antibodies for horseradish peroxidase–conjugated goat were detected using Chemiluminescent detection Amersham ECL Advance Western Blotting Detection Kit (Amersham Biosciences; catalog no.: RPN2135), and subsequent autoradiography was applied to visualize bands. A densitometric scan of the films was used to quantify the results. For analyzing, ImageJ (rasband, W.S. imageJ; National Institute of health) was used to measure the integrated density of bands after background subtraction. The Western blot analysis was done at least twice.

Statistical analysis

All the experiments were done at least three times, and the final data are represented as the mean ± SEM. Data were analyzed using PRISM 8 (GraphPad Software, Inc). One-way ANOVA followed by Turkey's post hoc test was used to analyze the differences between groups. *t* Test was used when two independent groups were compared to analyze the difference. Statistical significance was defined at $p < 0.05$.

Data availability

All data are contained within the article.

Acknowledgments—We thank all staff of the cellular biotechnology department at Royan institute and our colleagues at Isfahan University.

Author contributions—S. B.-A. and F. K. conceptualization; S. B.-A. methodology; S. B.-A. and F. K. validation; S. B.-A. formal analysis; S. B.-A. and F. K. investigation; S. B.-A. resources; F. K. data curation; S. B.-A. writing–original draft; M. H. N.-E. writing–reviewing & editing; F. K. visualization; M. H. N.-E. supervision; M. H. N.-E. project administration; M. H. N.-E. funding acquisition.

Funding and additional information—This work was supported by a grant from Iran National Science Foundation (grant number: 98020517) to M. H. N.-E, as the principal investigator; this study was also partly supported by the University of Isfahan to help S. B.-A. to get her PhD.

Conflict of interest—The authors declare that they have no conflicts of interest with the contents of this article.

Abbreviations—The abbreviations used are: ALP, alkaline phosphatase; DFO, deferoxamine; Fer-1, ferrostatin-1; GPX4, glutathione peroxidase 4; hESC, human embryonic stem cell; MDA, malondialdehyde; MTS, (3-(4,5-dimethylthiazol-2-yl)-2,5-diphenyltetrazolium bromide; Nrf2, nuclear factor erythroid 2–related factor 2; Pft-α, pifithrin α; PUFA, polyunsaturated fatty acid; qRT–PCR, quantitative RT–PCR; ROCK, Rho kinase; ROS, reactive oxygen species; xCT, the cystine–glutamate antiporter.

References

1. Thomson, J. A., Itskovitz-Eldor, J., Shapiro, S. S., Waknitz, M. A., Swiergiel, J. J., Marshall, V. S., and Jones, J. M. (1998) Embryonic stem cell lines derived from human blastocysts. *Science* **282**, 1145–1147
2. Takahashi, K., and Yamanaka, S. (2006) Induction of pluripotent stem cells from mouse embryonic and adult fibroblast cultures by defined factors. *Cell* **126**, 663–676
3. Musunuru, K., Domian, I. J., and Chien, K. R. (2010) Stem cell models of cardiac development and disease. *Annu. Rev. Cell Dev. Biol.* **26**, 667–687
4. Masuda, S., Miyagawa, S., Fukushima, S., Nakamura, T., Khurram, M. A., Ishikawa, T., Saito, A., and Sawa, Y. (2016) Expandable progenitors from induced pluripotent stem cells. *Nat. Rev. Cardiol.* **13**, 574
5. Lei, Y., and Schaffer, D. V. (2013) A fully defined and scalable 3D culture system for human pluripotent stem cell expansion and differentiation. *Proc. Natl. Acad. Sci. U. S. A.* **110**, E5039–5048
6. Wu, Y., Shu, J., He, C., Li, M., Wang, Y., Ou, W., and He, Y. (2016) ROCK inhibitor Y27632 promotes proliferation and diminishes apoptosis of marmoset induced pluripotent stem cells by suppressing expression and activity of caspase 3. *Theriogenology* **85**, 302–314
7. Brown, C. W., Amante, J. J., and Mercurio, A. M. (2018) Cell clustering mediated by the adhesion protein PVRL4 is necessary for alpha6beta4 integrin-promoted ferroptosis resistance in matrix-detached cells. *J. Biol. Chem.* **293**, 12741–12748

8. Brown, C. W., Amante, J. J., Goel, H. L., and Mercurio, A. M. (2017) The alpha6beta4 integrin promotes resistance to ferroptosis. *J. Cell Biol.* **216**, 4287–4297
9. Dixon, S. J., Lemberg, K. M., Lamprecht, M. R., Skouta, R., Zaitsev, E. M., Gleason, C. E., Patel, D. N., Bauer, A. J., Cantley, A. M., Yang, W. S., Morrison, B., 3rd, and Stockwell, B. R. (2012) Ferroptosis: An iron-dependent form of nonapoptotic cell death. *Cell* **149**, 1060–1072
10. Gao, M., Monian, P., Quadri, N., Ramasamy, R., and Jiang, X. (2015) Glutaminolysis and transferrin regulate ferroptosis. *Mol. Cell* **59**, 298–308
11. Yang, W. S., Kim, K. J., Gaschler, M. M., Patel, M., Shchepinov, M. S., and Stockwell, B. R. (2016) Peroxidation of polyunsaturated fatty acids by lipoxygenases drives ferroptosis. *Proc. Natl. Acad. Sci. U. S. A.* **113**, E4966–E4975
12. Doll, S., Proneth, B., Tyurina, Y. Y., Panzilius, E., Kobayashi, S., Ingold, I., Irmler, M., Beckers, J., Aichler, M., Walch, A., Prokisch, H., Trumbach, D., Mao, G., Qu, F., Bayir, H., *et al.* (2017) ACSL4 dictates ferroptosis sensitivity by shaping cellular lipid composition. *Nat. Chem. Biol.* **13**, 91–98
13. Sperber, H., Mathieu, J., Wang, Y., Ferreccio, A., Hesson, J., Xu, Z., Fischer, K. A., Devi, A., Detraux, D., Gu, H., Battle, S. L., Showalter, M., Valensisi, C., Bielas, J. H., Ericson, N. G., *et al.* (2015) The metabolome regulates the epigenetic landscape during naive-to-primed human embryonic stem cell transition. *Nat. Cell Biol.* **17**, 1523–1535
14. Liu, J. C., Guan, X., Ryan, J. A., Rivera, A. G., Mock, C., Agrawal, V., Letai, A., Lerou, P. H., and Lahav, G. (2013) High mitochondrial priming sensitizes hESCs to DNA-damage-induced apoptosis. *Cell Stem Cell* **13**, 483–491
15. Setoguchi, K., TeSlaa, T., Koehler, C. M., and Teitell, M. A. (2016) P53 regulates rapid apoptosis in human pluripotent stem cells. *J. Mol. Biol.* **428**, 1465–1475
16. Angeli, J. P. F., Shah, R., Pratt, D. A., and Conrad, M. (2017) Ferroptosis inhibition: Mechanisms and opportunities. *Trends Pharmacol. Sci.* **38**, 489–498
17. Xie, Y., Hou, W., Song, X., Yu, Y., Huang, J., Sun, X., Kang, R., and Tang, D. (2016) Ferroptosis: Process and function. *Cell Death Differ.* **23**, 369–379
18. Liu, Z., Lv, X., Song, E., and Song, Y. (2020) Fostered Nrf2 expression antagonizes iron overload and glutathione depletion to promote resistance of neuron-like cells to ferroptosis. *Toxicol. Appl. Pharmacol.* **407**, 115241
19. La Rosa, P., Petrillo, S., Turchi, R., Berardinelli, F., Schirinzi, T., Vasco, G., Lettieri-Barbato, D., Fiorenza, M. T., Bertini, E. S., Aquilano, K., and Piemonte, F. (2021) The Nrf2 induction prevents ferroptosis in Friedreich's Ataxia. *Redox Biol.* **38**, 101791
20. Mbah, N. E., and Lyssiotis, C. A. (2022) Metabolic regulation of ferroptosis in the tumor microenvironment. *J. Biol. Chem.* **298**, 101617
21. Dixon, S. J., and Stockwell, B. R. (2014) The role of iron and reactive oxygen species in cell death. *Nat. Chem. Biol.* **10**, 9–17
22. Friedmann Angeli, J. P., Schneider, M., Proneth, B., Tyurina, Y. Y., Tyurin, V. A., Hammond, V. J., Herbach, N., Aichler, M., Walch, A., Eggenhofer, E., Basavarajappa, D., Radmark, O., Kobayashi, S., Seibt, T., Beck, H., *et al.* (2014) Inactivation of the ferroptosis regulator Gpx4 triggers acute renal failure in mice. *Nat. Cell Biol.* **16**, 1180–1191
23. Lo, M., Wang, Y. Z., and Gout, P. W. (2008) The x(c)- cystine/glutamate antiporter: A potential target for therapy of cancer and other diseases. *J. Cell Physiol.* **215**, 593–602
24. Qin, H., Yu, T., Qing, T., Liu, Y., Zhao, Y., Cai, J., Li, J., Song, Z., Qu, X., Zhou, P., Wu, J., Ding, M., and Deng, H. (2007) Regulation of apoptosis and differentiation by p53 in human embryonic stem cells. *J. Biol. Chem.* **282**, 5842–5852
25. Xu, X., Cowley, S., Flaim, C. J., James, W., Seymour, L., and Cui, Z. (2010) The roles of apoptotic pathways in the low recovery rate after cryopreservation of dissociated human embryonic stem cells. *Biotechnol. Prog.* **26**, 827–837
26. Yang, W. S., SriRamaratnam, R., Welsch, M. E., Shimada, K., Skouta, R., Viswanathan, V. S., Cheah, J. H., Clemons, P. A., Shamji, A. F., Clish, C. B., Brown, L. M., Girotti, A. W., Cornish, V. W., Schreiber, S. L., and Stockwell, B. R. (2014) Regulation of ferroptotic cancer cell death by GPX4. *Cell* **156**, 317–331
27. Jiang, L., Kon, N., Li, T., Wang, S. J., Su, T., Hibshoosh, H., Baer, R., and Gu, W. (2015) Ferroptosis as a p53-mediated activity during tumour suppression. *Nature* **520**, 57–62
28. Zhang, L., Ma, L., Yan, T., Han, X., Xu, J., Xu, J., and Xu, X. (2018) Activated mitochondrial apoptosis in hESCs after dissociation involving the PKA/p-p53/Bax signaling pathway. *Exp. Cell Res.* **369**, 226–233
29. Fan, Z., Wirth, A. K., Chen, D., Wruck, C. J., Rauh, M., Buchfelder, M., and Savaskan, N. (2017) Nrf2-Keap1 pathway promotes cell proliferation and diminishes ferroptosis. *Oncogenesis* **6**, e371
30. Yang, W. S., and Stockwell, B. R. (2008) Synthetic lethal screening identifies compounds activating iron-dependent, nonapoptotic cell death in oncogenic-RAS-harboring cancer cells. *Chem. Biol.* **15**, 234–245
31. Han, Z., Xu, Z., Chen, L., Ye, D., Yu, Y., Zhang, Y., Cao, Y., Djibril, B., Guo, X., Gao, X., Zhang, W., Yu, M., Liu, S., Yan, G., Jin, M., *et al.* (2020) Iron overload inhibits self-renewal of human pluripotent stem cells via DNA damage and generation of reactive oxygen species. *FEBS Open Bio.* **10**, 726–733
32. Han, Z., Yu, Y., Xu, J., Bao, Z., Xu, Z., Hu, J., Yu, M., Bamba, D., Ma, W., Ding, F., Zhang, L., Jin, M., Yan, G., Huang, Q., Wang, X., *et al.* (2019) Iron homeostasis determines fate of human pluripotent stem cells via Glycerophospholipids-epigenetic circuit. *Stem Cells* **37**, 489–503
33. Yu, H., Guo, P., Xie, X., Wang, Y., and Chen, G. (2017) Ferroptosis, a new form of cell death, and its relationships with tumourous diseases. *J. Cell Mol. Med.* **21**, 648–657
34. Dodson, M., Castro-Portuguez, R., and Zhang, D. D. (2019) NRF2 plays a critical role in mitigating lipid peroxidation and ferroptosis. *Redox Biol.* **23**, 101107
35. Watanabe, K., Ueno, M., Kamiya, D., Nishiyama, A., Matsumura, M., Wataya, T., Takahashi, J. B., Nishikawa, S., Nishikawa, S., Muguruma, K., and Sasai, Y. (2007) A ROCK inhibitor permits survival of dissociated human embryonic stem cells. *Nat. Biotechnol.* **25**, 681–686
36. Ohgushi, M., Matsumura, M., Eiraku, M., Murakami, K., Aramaki, T., Nishiyama, A., Muguruma, K., Nakano, T., Suga, H., Ueno, M., Ishizaki, T., Suemori, H., Narumiya, S., Niwa, H., and Sasai, Y. (2010) Molecular pathway and cell state responsible for dissociation-induced apoptosis in human pluripotent stem cells. *Cell Stem Cell* **7**, 225–239
37. Zhang, L., Xu, Y., Xu, J., Wei, Y., and Xu, X. (2016) Protein kinase A inhibitor, H89, enhances survival and clonogenicity of dissociated human embryonic stem cells through Rho-associated coiled-coil containing protein kinase (ROCK) inhibition. *Hum. Reprod.* **31**, 832–843
38. Frisch, S. M., and Screaton, R. A. (2001) Anoikis mechanisms. *Curr. Opin. Cell Biol.* **13**, 555–562
39. Sun, X., Ou, Z., Xie, M., Kang, R., Fan, Y., Niu, X., Wang, H., Cao, L., and Tang, D. (2015) HSPB1 as a novel regulator of ferroptotic cancer cell death. *Oncogene* **34**, 5617–5625
40. El Hout, M., Dos Santos, L., Hamai, A., and Mehrpour, M. (2018) A promising new approach to cancer therapy: Targeting iron metabolism in cancer stem cells. *Semin. Cancer Biol.* **53**, 125–138
41. Wang, S. J., Ou, Y., Jiang, L., and Gu, W. (2016) Ferroptosis: A missing puzzle piece in the p53 blueprint? *Mol. Cell Oncol.* **3**, e1046581
42. Gnanapradeepan, K., Basu, S., Barnoud, T., Budina-Kolomets, A., Kung, C. P., and Murphy, M. E. (2018) The p53 tumor suppressor in the control of metabolism and ferroptosis. *Front. Endocrinol. (Lausanne)* **9**, 124
43. Liu, J., Zhang, C., Hu, W., and Feng, Z. (2019) Tumor suppressor p53 and metabolism. *J. Mol. Cell Biol.* **11**, 284–292
44. Funauchi, Y., Tanikawa, C., Yi Lo, P. H., Mori, J., Daigo, Y., Takano, A., Miyagi, Y., Okawa, A., Nakamura, Y., and Matsuda, K. (2015) Regulation of iron homeostasis by the p53-ISCU pathway. *Sci. Rep.* **5**, 16497
45. Chen, M. J., Chou, C. H., Shun, C. T., Mao, T. L., Wen, W. F., Chen, C. D., Chen, S. U., Yang, Y. S., and Ho, H. N. (2017) Iron suppresses ovarian granulosa cell proliferation and arrests cell cycle through regulating p38 mitogen-activated protein kinase/p53/p21 pathway. *Biol. Reprod.* **97**, 438–448

46. Dai, X., Yan, X., Wintergerst, K. A., Cai, L., Keller, B. B., and Tan, Y. (2020) Nrf2: Redox and metabolic regulator of stem cell state and function. *Trends Mol. Med.* **26**, 185–200
47. Rapoport, T. A. (1991) Protein transport across the endoplasmic reticulum membrane: Facts, models, mysteries. *FASEB J.* **5**, 2792–2798
48. Nguyen, T., Nioi, P., and Pickett, C. B. (2009) The Nrf2-antioxidant response element signaling pathway and its activation by oxidative stress. *J. Biol. Chem.* **284**, 13291–13295
49. Viswanathan, V. S., Ryan, M. J., Dhruv, H. D., Gill, S., Eichhoff, O. M., Seashore-Ludlow, B., Kaffenberger, S. D., Eaton, J. K., Shimada, K., Aguirre, A. J., Viswanathan, S. R., Chattopadhyay, S., Tamayo, P., Yang, W. S., Rees, M. G., *et al.* (2017) Dependency of a therapy-resistant state of cancer cells on a lipid peroxidase pathway. *Nature* **547**, 453–457
50. Dixon, S. J., Patel, D. N., Welsch, M., Skouta, R., Lee, E. D., Hayano, M., Thomas, A. G., Gleason, C. E., Tatonetti, N. P., Slusher, B. S., and Stockwell, B. R. (2014) Pharmacological inhibition of cystine-glutamate exchange induces endoplasmic reticulum stress and ferroptosis. *Elife* **3**, e02523
51. Yant, L. J., Ran, Q., Rao, L., Van Remmen, H., Shibatani, T., Belter, J. G., Motta, L., Richardson, A., and Prolla, T. A. (2003) The selenoprotein GPX4 is essential for mouse development and protects from radiation and oxidative damage insults. *Free Radic. Biol. Med.* **34**, 496–502
52. Jang, J., Wang, Y., Kim, H. S., Lalli, M. A., and Kosik, K. S. (2014) Nrf2, a regulator of the proteasome, controls self-renewal and pluripotency in human embryonic stem cells. *Stem Cells* **32**, 2616–2625
53. Sart, S., Song, L., and Li, Y. (2015) Controlling redox status for stem cell survival, expansion, and differentiation. *Oxid. Med. Cell Longev.* **2015**, 105135
54. Ishii, T., and Mann, G. E. (2014) Redox status in mammalian cells and stem cells during culture *in vitro*: Critical roles of Nrf2 and cystine transporter activity in the maintenance of redox balance. *Redox Biol.* **2**, 786–794
55. Sato, H., Tamba, M., Ishii, T., and Bannai, S. (1999) Cloning and expression of a plasma membrane cystine/glutamate exchange transporter composed of two distinct proteins. *J. Biol. Chem.* **274**, 11455–11458
56. Jin, L., Ni, J., Tao, Y., Weng, X., Zhu, Y., Yan, J., and Hu, B. (2019) N-acetylcysteine attenuates PM2.5-induced apoptosis by ROS-mediated Nrf2 pathway in human embryonic stem cells. *Sci. Total Environ.* **666**, 713–720
57. Bannai, S. (1984) Transport of cystine and cysteine in mammalian cells. *Biochim. Biophys. Acta* **779**, 289–306
58. Barradas, M. A., Jeremy, J. Y., Kontoghiorghes, G. J., Mikhailidis, D. P., Hoffbrand, A. V., and Dandona, P. (1989) Iron chelators inhibit human platelet aggregation, thromboxane A2 synthesis and lipoxygenase activity. *FEBS Lett.* **245**, 105–109
59. Baharvand, H., Ashtiani, S. K., Taee, A., Massumi, M., Valojerdi, M. R., Yazdi, P. E., Moradi, S. Z., and Farrokhi, A. (2006) Generation of new human embryonic stem cell lines with diploid and triploid karyotypes. *Dev. Growth Differ.* **48**, 117–128
60. Ellman, G. L. (1959) Tissue sulfhydryl groups. *Arch. Biochem. Biophys.* **82**, 70–77
61. Schmittgen, T. D., and Livak, K. J. (2008) Analyzing real-time PCR data by the comparative C(T) method. *Nat. Protoc.* **3**, 1101–1108
62. Bradford, M. M. (1976) A rapid and sensitive method for the quantitation of microgram quantities of protein utilizing the principle of protein-dye binding. *Anal. Biochem.* **72**, 248–254